12-14-89 JSO

UCID-21619

Design of a Custom Load Cell for a Precision Assembly Application

John J. Scott

October 25, 1989

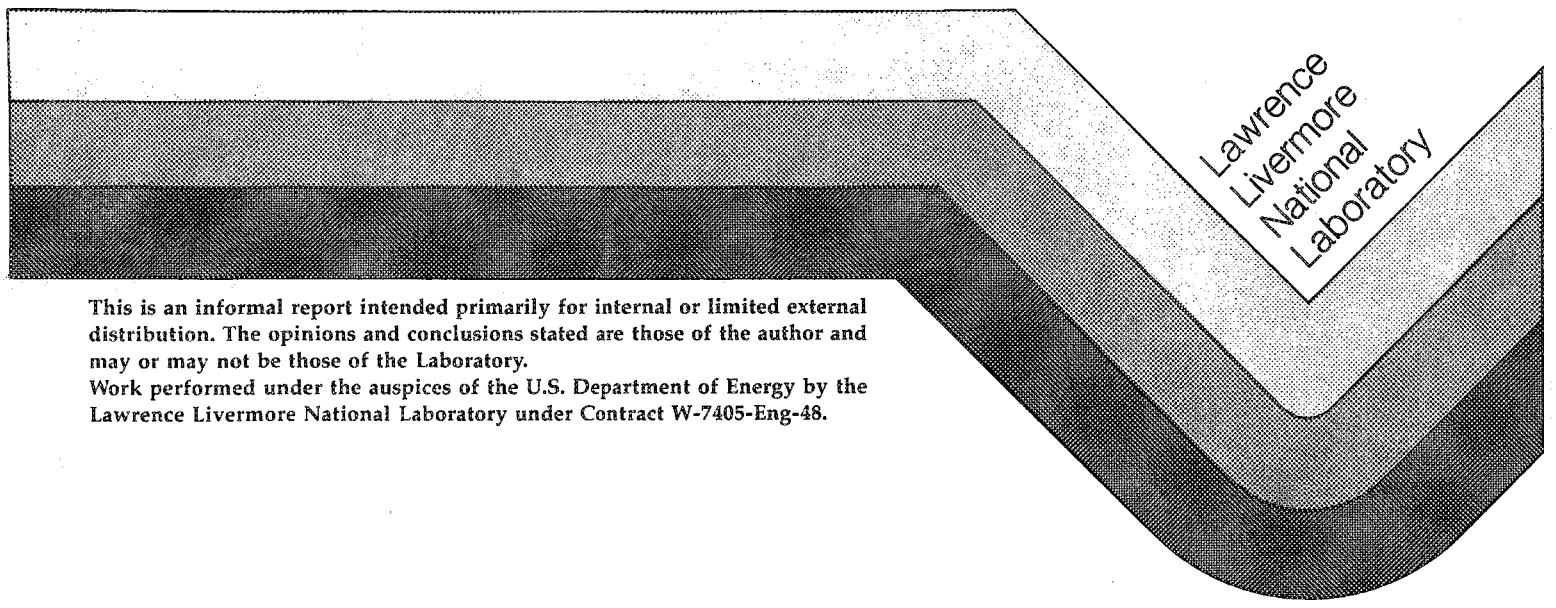

This report has been reproduced
directly from the best available copy.

Available to DOE and DOE contractors from the
Office of Scientific and Technical Information
P.O. Box 62, Oak Ridge, TN 37831
Prices available from (615) 576-8401, FTS 626-8401.

Available to the public from the
National Technical Information Service
U.S. Department of Commerce
5285 Port Royal Rd.,
Springfield, VA 22161

Price Code	Page Range
A01	Microfiche
Papercopy Prices	
A02	001-050
A03	051-100
A04	101-200
A05	201-300
A06	301-400
A07	401-500
A08	501-600
A09	601

UCID--21619

DE90 004439

Table of Contents

Design of a Custom Load Cell for a Precision Assembly Application

Abstract

A custom load cell was designed for a precision assembly application where high sensitivity and minimum deflections were required in two orthogonal directions. The application required that the load cell be integrated into existing micropositioning equipment. The aluminum alloy 2024-T81 was used as the spring material to maximize both strain output and gage heat dissipation. Large area, high resistance gages were selected to minimize heat generation and maximize dissipation. Dual Wheatstone bridge circuits were used to resolve the two orthogonal directions. The spring element was designed for optimal mechanical sensitivity, heat dissipation, and ease of fabrication. The described hardware was fabricated and successfully used to support a major LLNL research program.

This paper was written as a case study to benefit future designers of such hardware.

Introduction

We designed the custom load cell described in this report for a research program at LLNL that requires the precise installation and alignment of experiments into a two-dimensional, rigid-body array. Individual experiments are mounted on a single, linear foundation, known as shelves. The shelves are mounted on a larger platform, known as a strongback, in a prescribed geometric pattern. During installation, the individual shelves must be positioned in predetermined locations to high accuracy (±0.000250 in.). Once in position, attachment screws are tightened to secure each shelf. These screws pass through a clearance hole in each end of the shelf and thread into the strongback. Approximate dimensions for shelves are 2 in. tall × 0.75 in. wide × 40 in. long. The fiber-composite shelves have a modulus approximately equal to aluminum (about 10×10^6 psi) with limited cross-sectional moment. The shelves can easily be distorted (bowed, twisted, etc.) if excessive end loads or lateral forces are applied during installation. To avoid applying such forces, a load cell was designed to be an integral part of the micropositioning hardware.

Figure 1 shows the longitudinal (end) and lateral (side) loads applied by the micropositioning hardware. Also shown in this figure is the detail of micropositioner engagement with the shelf. The two mating surfaces form a two-dimensional ball and socket joint. Compliant longitudinal loading of these interfaces eliminates lateral sideplay, thus permitting precise micropositioning. Longitudinal positioning of a shelf is maintained by the rigid vertical arm while compliant loading is achieved by "pushing" with the opposite compliant vertical arm. When approximately 0.012 in. of elastic top-to-bottom deflection is achieved, the compliant arm is shaped like a parallelogram and exerts the required end load of 1.0 lb. With the proper pressure applied, the shelves are then micropositioned laterally and secured.

In addition to setting and measuring the desired longitudinal end load of approximately 1.0 lb, the load cell also monitors lateral loads during micropositioning to ensure that they remain less than 0.1 lb. Due to the iterative nature of the installation process, the screws are tightened and released many times. If a screw is inadvertently left tightened, or if the clearance between the shelf and the screw is lost (through interference), excessive lateral loads would be applied to the shelf or strongback. The load cell monitors both longitudinal and lateral loads to ensure that excess loads are not applied.

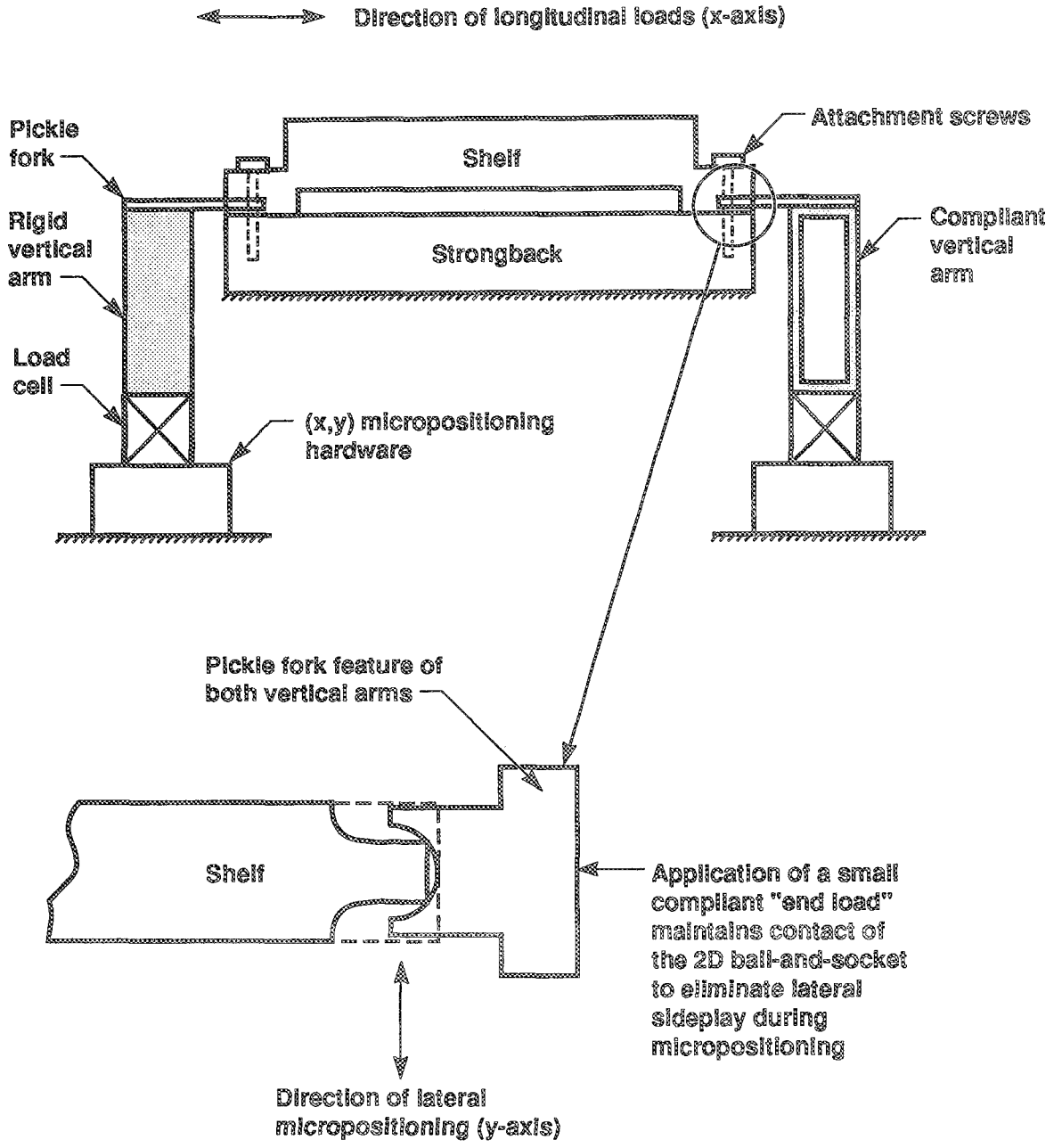

Figure 1. A conceptual drawing of the application.

Electrical Design Considerations

Wheatstone Bridge Options

Only conventional Wheatstone bridge electrical circuits were considered. Our selected instrumentation is a high impedance voltage measuring device that is currently popular for such applications. The voltage solution for a Wheatstone bridge is detailed in Appendix A.

Figure 2 shows the three bridge wiring options considered. Option 1 shows how the two orthogonal directions could be measured using only two active gages per bridge. Since each bridge requires four resistances, two "dummy" (inactive) resistances must be added. The best way to do this is to place identical gages in an unstrained area of the load cell. Option 1 uses a total of eight gages which must be purchased, installed and wired. Since bridge output is proportional to the number of *active* gages, option 1 supplies only half the output of 2 and 3, yet costs just as much to implement. It would be of interest only if space were critical and only four gages could be located on the strained surface of the spring perimeter. Since space was not a problem and maximum output was required, option 1 was rejected.

In options 2 and 3, all gages are active and thus form bridges with maximum output signal. In option 2, all four gages for a given force direction are located on the neutral axis of the orthogonal force. In theory, the signal crosstalk between orthogonal forces is eliminated by the neutral axis placement. In option 3, all gages appear in the strain fields of both orthogonal forces. In this configuration, signal crosstalk is counteracted in the bridge by equal orthogonally induced strains. Both options 2 and 3 were considered to be acceptable electrical designs. Later mechanical design optimizations resulted in the selection of option 3.

Strain Gage Selection

There are basically two types of strain gages

- Standard metal foil or wire gages
- Semiconductor (piezoresistance) gages

Semiconductor gages, at first, would seem to be the best choice for any strain gage application. Metal gages have gage output factors of only two to four, while semiconductor gages typically have factors of 45–200. For a given strain, the output signal is much greater. Also, semiconductor gages accept greater excitation voltage with less heat dissipation. Therefore, they produce a further increase in output signal. However, semiconductor gages are seldom used. A closer examination reveals why:

Cost - Semiconductor gages cost 7 to 20 times that of a foil gage.

Temperature Compensation - Semiconductor gages are PN crystals which do not offer great flexibility in fabrication variation. They cannot be well matched to coefficient of thermal expansion (CTE) induced apparent strain or other temperature effects on gage factor, resistance, or linearity, as can metallic gages.

Technology - Ironically, it is the new technology of semiconductor electronics that makes semiconductor gages less advantageous. Semiconductor instrumentation can now easily detect the lower output levels of conventional metallic gages.

Hysteresis - There are practical limits on the smallest unit of resolution (strain) that can be measured. The author was advised by more than one experienced individual not to attempt resolution below one microstrain (0.000001 in. per in.). Both semiconductor and foil gages have this same hysteresis limitation.

Therefore, a conventional metallic foil gage was selected for this application—specifically a MicroEngineering 250BA-1000. The specifications for this strain gate are documented in Appendix B. This particular

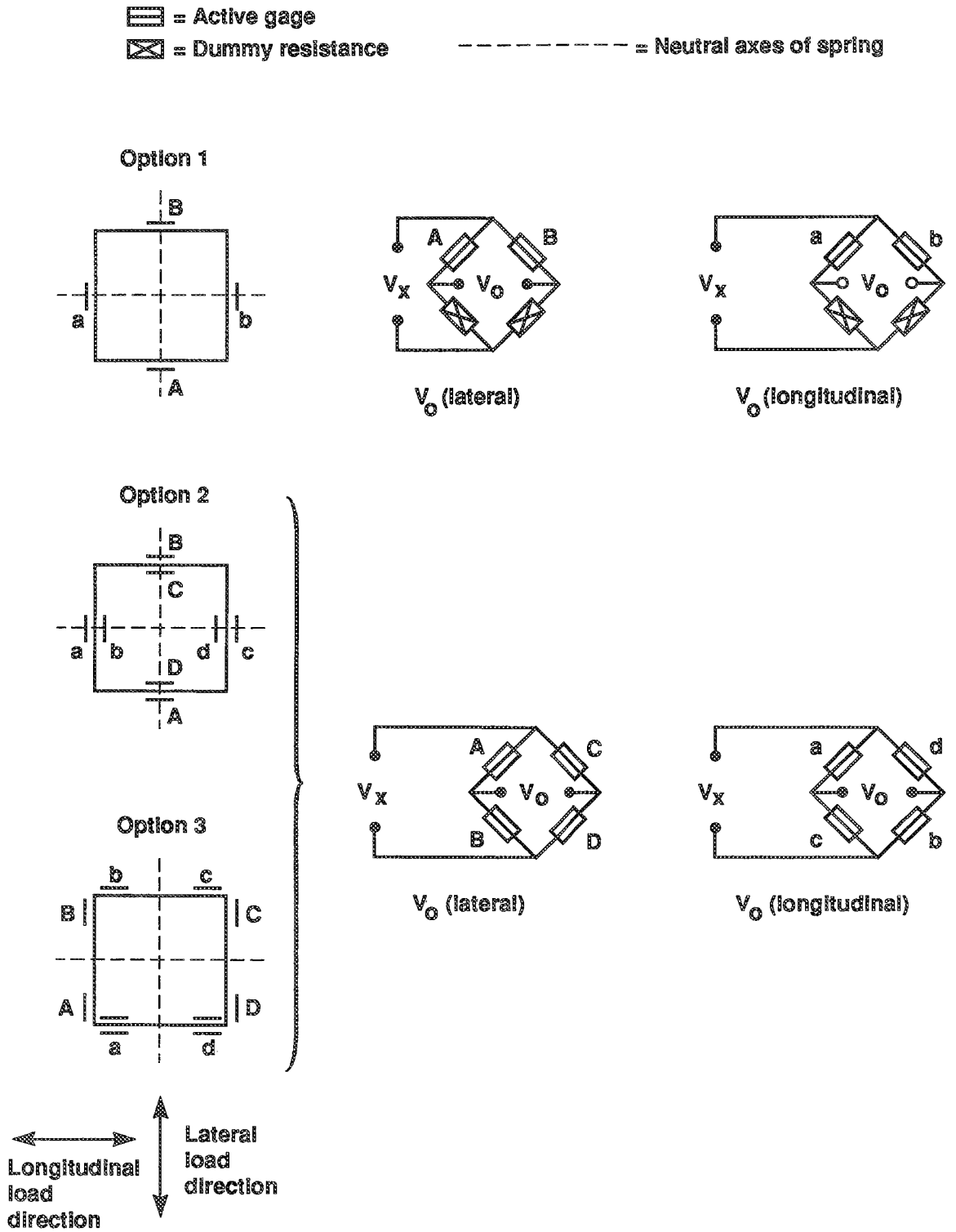

Figure 2. Three Wheatstone bridge wiring options.

gage was selected because its relatively high resistance (1000 ohms) is valuable for minimal heat generation and its large grid area (0.125 in. wide × 0.250 in. long) for maximal heat dissipation. Also, this gage was available with an aluminum CTE compensation to match the spring material.

For high accuracy on an *aluminum* heat sink, it is recommended that power density (heat dissipation per unit area) not exceed 1.-1.5 W/in² [Ref. 1]. Power density is calculated in the following manner:

Since $P = \frac{V^2}{R} = \frac{5^2}{1000} = 0.025$ W

where: Gage voltage = 5 V (10 V for bridge)

Gage area = 0.0313 in.² (0.125 × .250)

Gage resistance = 1000. ohms

then Power density $= \frac{P}{\text{area}} = \frac{.025}{0.0313} = 0.8$ W/in.²

These calculations were repeated many times to show that smaller grid sizes and/or lower resistance gages could not be used. The reader must also note that the high thermal conductivity of an aluminum spring was assumed for these calculations. This is important to the discussion of material selection.

Once the electrical requirements were determined, the physical size of the selected strain gage was known and became a consideration in the design of the load cell. For the benefit of the reader, some strain-gage size terms are defined.

Grid - The small part of the foil pattern with the thin elements that actually detect strain. To most manufacturers the terms *grid* and *gage* are synonymous. Thus, grid length (width) is also called gage length (width).

Pattern - The total (overall) size of the foil pattern including the solder tabs. The terms *pattern* and *overall* are synonymous. Pattern length and gage length are *not* the same and are often confused.

Backing Material - The foil pattern resides on a nonconductive backing material. Excess backing material is usually trimmed away prior to use. Trimming may be as close as .010 in. to the pattern without affecting the gage.

Matrix - Matrix is a confusing term and readers should be aware of the definition in use. Some people refer to matrix as the size of the trimmed backing material. Others refer to matrix as the rectangular dimensions defined by trim marks around the gage pattern(s). The two definitions are synonymous if trimming is done to the trim marks. This latter definition is more useful for patterns containing multiple gages.

Mechanical Design Considerations

Design Objectives

The mechanical design of the load cell and its integration into the existing micropositioning hardware was the most challenging aspect of this project. In designing the load cell, we were mindful of the following electrical and mechanical requirements:

- Maximum sensitivity
  Minimum resolvable force = 0.02 lb (lateral direction)
  Nominal applied force = 1.0 lb (longitudinal direction)
- Maximum resistance to overload
- Cost of mechanical fabrication
- Ease of mounting and wiring gages
- Monolithic construction—In load cell design, it is best to make the spring element out of a single piece of material. Weldments, brazing, and bolted connections are undesirable.
- Space requirement for eight gages—The two bridge circuits required a uniformly strained surface area for eight rather large gages.
- Symmetry requirements for gage sets—The four gages in each bridge circuit were to be symmetrically located about the intersection of the two orthogonal neutral axes.
- Minimum deflection under load—The process of micropositioning to high accuracy is difficult when there are excessive elastic deflections due to applied loads.

Figure 3 is an early conceptual sketch of the mechanical design. The load cell system consists of two separate parts: the upper portion, a vertical lever arm with a "pickle fork" feature that actually contacts and positions the shelf (the pickle fork is the micropositioning driver of the two-dimensional ball-and-socket scheme discussed earlier), and the lower portion, the spring element which, when instrumented, will become the load cell.

We decided to use a vertical lever arm to transmit and mechanically amplify the orthogonal loads to a lower spring element. Besides making force magnification easy, the vertical arm concept also integrated well with the existing micropositioning hardware. The lever arm distance of approximately 5 in. was a compromise between mechanical advantage, resulting lateral deflection, and system integration. The next sections discuss the selection of 2024-T81 for the spring material, and the evolution and design optimization of the spring.

Material Selection for the Spring Element

The author was confronted with many conflicting requirements in selecting the best material for the spring element. The important design criteria for this selection process are identified and discussed below.

Young's Modulus

In load cell design the largest signal comes from the lowest modulus. The disadvantage of a low modulus is increased elastic deflections at the pickle fork. In this "micropositioning" application we wanted both high sensitivity and high rigidity, an obvious conflict of requirements. Aluminum, or another nonferrous metal, has a modulus less than steel but greater than plastics. Aluminum was a first guess as a compromise material. A possible alternative might be a fiber composite material with a matrix modulus approaching that of aluminum.

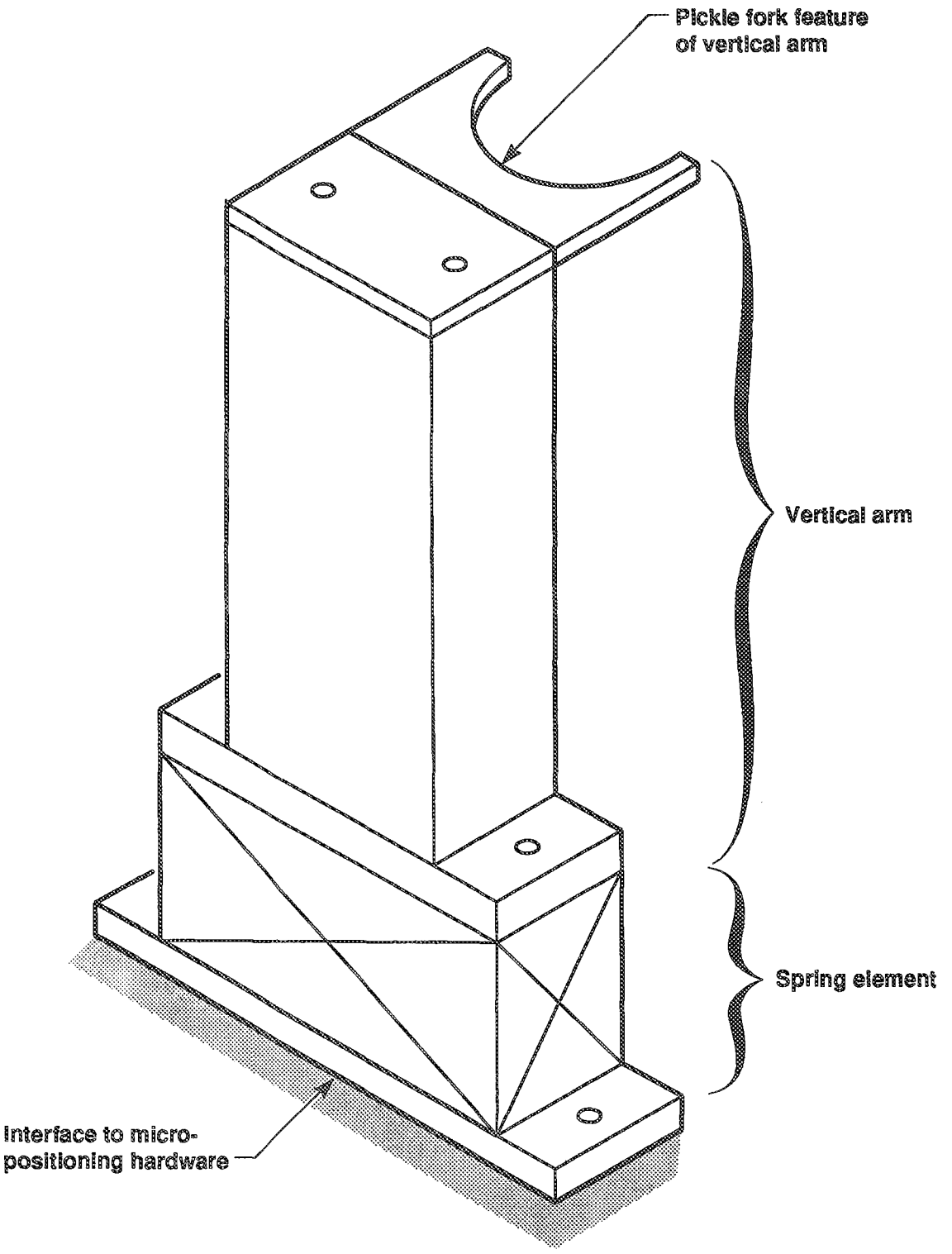

Figure 3. An early conceptual sketch of the load cell.

Yield Stress

Ideally, we would like to find a material with a stress-strain curve that runs off to infinity and never yields. Failing that, then for a given modulus, we desire the highest possible yield point. The higher the yield point (yield load) the less likely that the load cell will be damaged by an accidental overload.

Thermal Expansion Coefficient

This was not a significant issue for our application for several reasons

1. Our laboratory environment was temperature controlled to ±0.5°F.
2. A Wheatstone bridge with four identical gages offers inherent cancellation of temperature-induced effects.
3. We were able to purchase strain gages with a thermal expansion coefficient that matches aluminum.

Thermal Conductivity

Strain gages are resistors that generate heat. If the heat does not properly dissipate, the temperature of the gage will rise and its accuracy will suffer. Our requirement for maximum sensitivity suggests a maximum excitation voltage which, in turn, results in maximum heating. Once again we have conflicting requirements.

We can minimize the dissipation problem by selecting a material with high thermal conductivity. Aluminum is an excellent choice since its conductivity is greater than steel and much greater than plastic. This is one reason that a fiber composite might not be a good choice.

Linearity

Most engineers think of the stress-strain plot of Young's Modulus as a perfectly straight line. For real materials it is not straight. This is most important for users requiring high absolute accuracy (i.e., transducers, scales). For this application we were interested in differences from nominal so anything reasonable would work. From Appendix C, we see that our selected aluminum is almost as linear as the best grades of steel.

Hysteresis

In real materials, the stress-strain curve does not always return to a perfect zero. At zero load, the small amount of residual strain known as hysteresis results in a failure of the strain gage to return to a zero reading. Hysteresis can be present even after spring excitation to loads well below yield. This criterion is important when the resolution of small strains is desired, as it was in this application. Plastics were undesirable due to their problems with hysteresis. A metal was preferred. Aluminum alloy 2024-T81 was specifically selected because of its high resistance to hysteresis.

Machinability/Fabrication Cost

Aluminum is preferable to steel.

Corrosion Resistance

Aluminum and stainless steel are the two most popular choices.

Welding Considerations/Heat Treat

It is possible to make spring elements out of weldments. Often, it is necessary to follow welding with a heat treatment to restore desired mechanical properties. This can lead to distortion problems and/or requirements for subsequent machining. These were never issues for this application. We correctly believed that a design could be generated that would not require welding or brazing.

After sufficient deliberation we knew, for reasons of thermal conductivity and hysteresis, we wanted a metal, and not a plastic. Aluminum or another nonferrous metal was preferable to steel because of its lower modulus and greater thermal conductivity. The high performance of aluminum alloys gave us no reason to consider a different nonferrous metal. Of the various alloys described in Appendix C, we finally selected 2024-T81. Even though 6061-T6 is readily available at LLNL, the short delivery time and low raw material cost of 2024-T81 easily permitted our use of this premium transducer-quality alloy.

Conceptual Evolution of the Spring Element

Our next step was to generate a conceptual design for the spring element, one that could be refined to meet the necessary criteria. A solid rectangular beam (gauging the vertical arm) was an obvious first start. But, with its massive cross section, this shape is far too stiff to give sufficient strain. Considerably more creativity was needed.

Figure 4 shows a chronology of the evolution of the design of the spring cross section at the elevation of the gages. A hollow rectangular beam (Fig. 4a) was the next concept proposed. However, with a continuous perimeter, its wall thickness would need to be extremely thin (<0.010 in.) to give sufficient strain. Such a thin wall would not possess sufficient elastic stability and would pose problems in fabrication. Also, the continuous perimeter would make it difficult to gain access to the inner gages.

The next step was to concentrate all the strain under the gages by eliminating the ungaged perimeter. Using four rectangular feet (Fig. 4b) does this, and optimizes the design for maximum gage strain per unit load. We determined each foot would need to be 0.170 in. wide × 0.040 in. thick × 0.600 in. tall. The height and width were dictated by the size of the gage. These simple rectangular feet could not resist buckling in the thin direction. This problem, in turn, was solved by placing sufficient cross-sectional moment in both orthogonal directions (Fig. 4c). The 90° angle, L-shaped feet did this by maintaining foot-area at the expense of web thickness (now only 0.020 in.). With the corners pointing outward, there were eight symmetric (2 × 4) surfaces for the gages. While this was an optimal mechanical design , it did not meet the requirement for easy fabrication. By turning the corners inward (Fig. 4d), the spring could be fabricated as a monolithic structure by a series of end-mill machining operations. Figure 5 shows photos of the actual spring element.

This final configuration led to the selection of electrical option 3, since it, too, placed components near the corners of the spring element.

Optimization and Calculation of the Spring Element

Figure 6 is a photograph of the spring element, vertical arm, and pickle fork extension, while Fig. 7 shows the micropositioning hardware being used.

The strain gage selected has *pattern* dimensions of 0.125 in. wide × 0.375 in. long (*grid* dimensions of 0.125 in. wide × 0.250 in. long). This suggests matrix dimensions of at least .145 in. wide × .395 in. long. We decided a foot width of 0.170 in. ±0.005 in. would be acceptable for the combined tolerances of spring fabrication, backing material trimming, and gage installation (bonding). We planned to center the 0.250 in. grid length within the 0.600 in. of uniform foot height. This length of uniform strain area (i.e., constant cross-sectional area) was selected to minimize end effects, and to enable the inner solder tabs to rest on a flat surface.

Appendix D contains the simple calculations which worked very well to describe this spring. The equations were programmed into a computer spreadsheet application to enable an iterative design and optimization process. The computer output reflects the many parameters considered in the selected design. Results are shown in Table 1.

To achieve the required high degree of sensitivity, we limited the cross-sectional foot area (Wc) to .0064 in^2. Since the calculational results are linear with input (Applied Force Q), the following magnitudes are known:

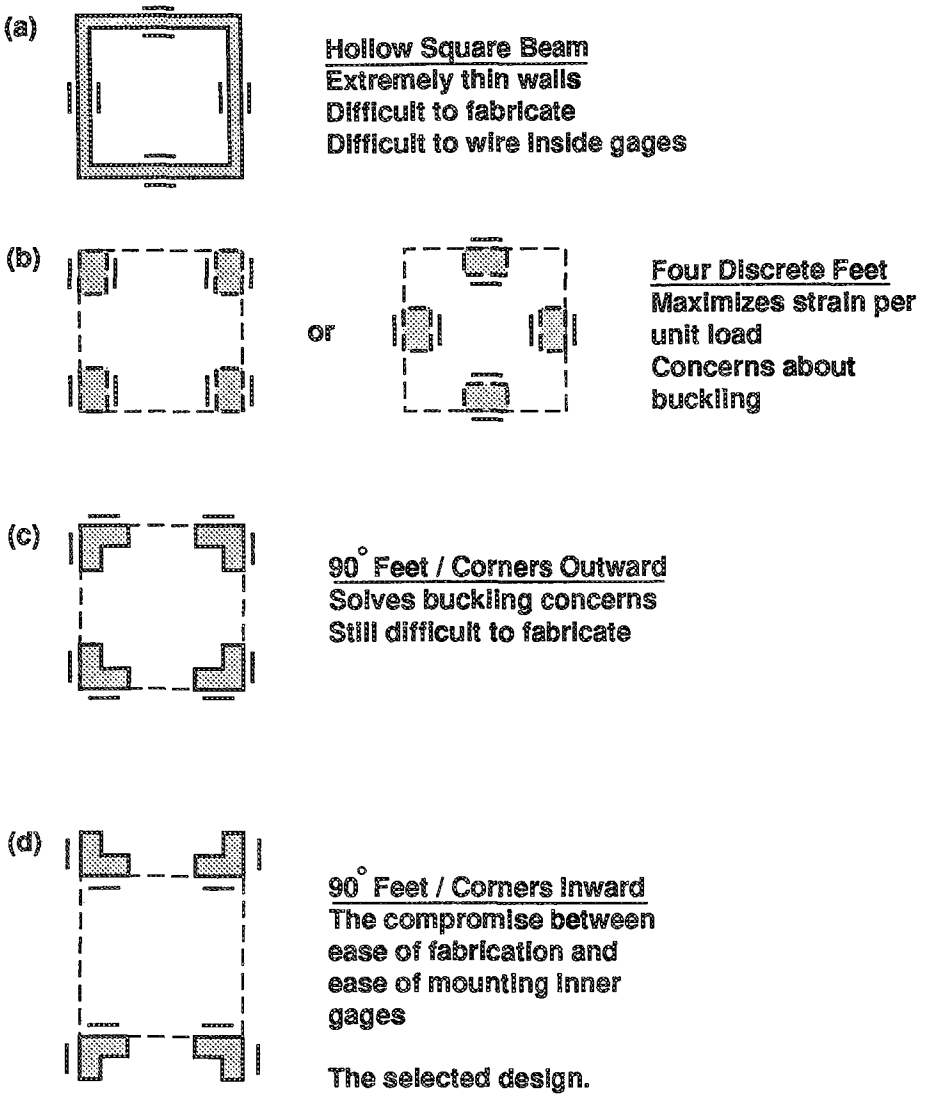

Figure 4. An evolution of the spring cross section.

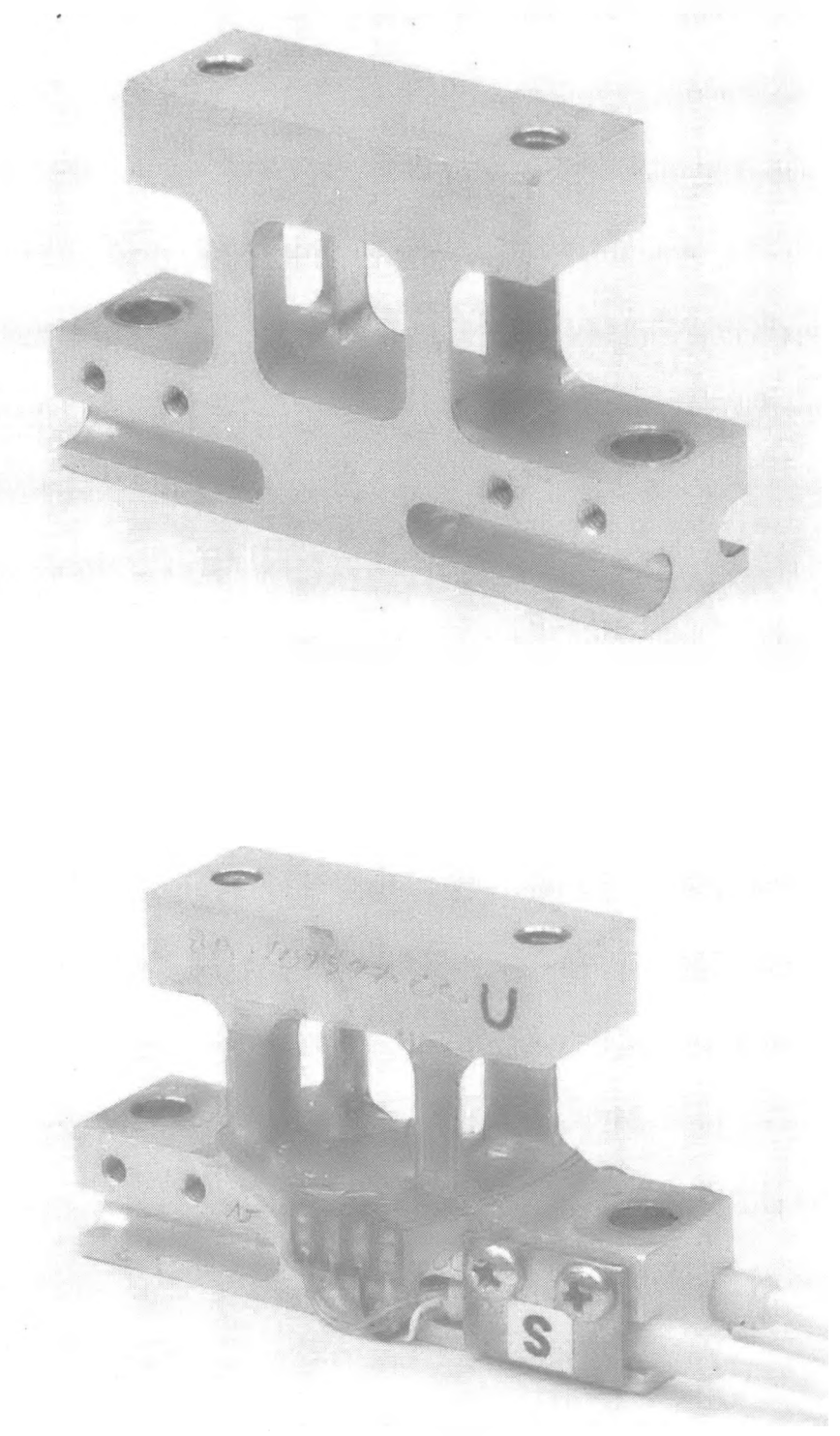

Figure 5. Photographs of the spring element.

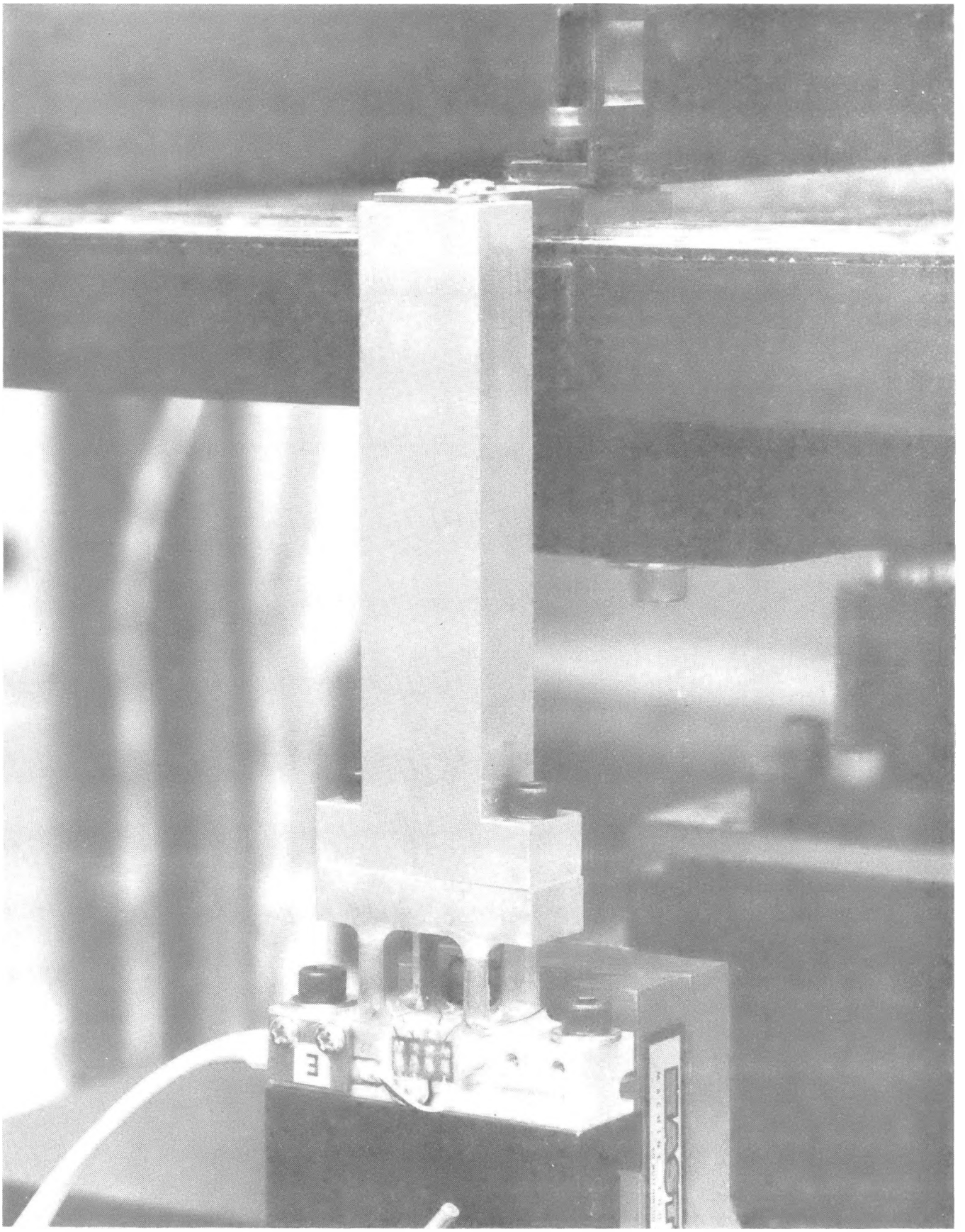

Figure 6. A photograph of the load cell.

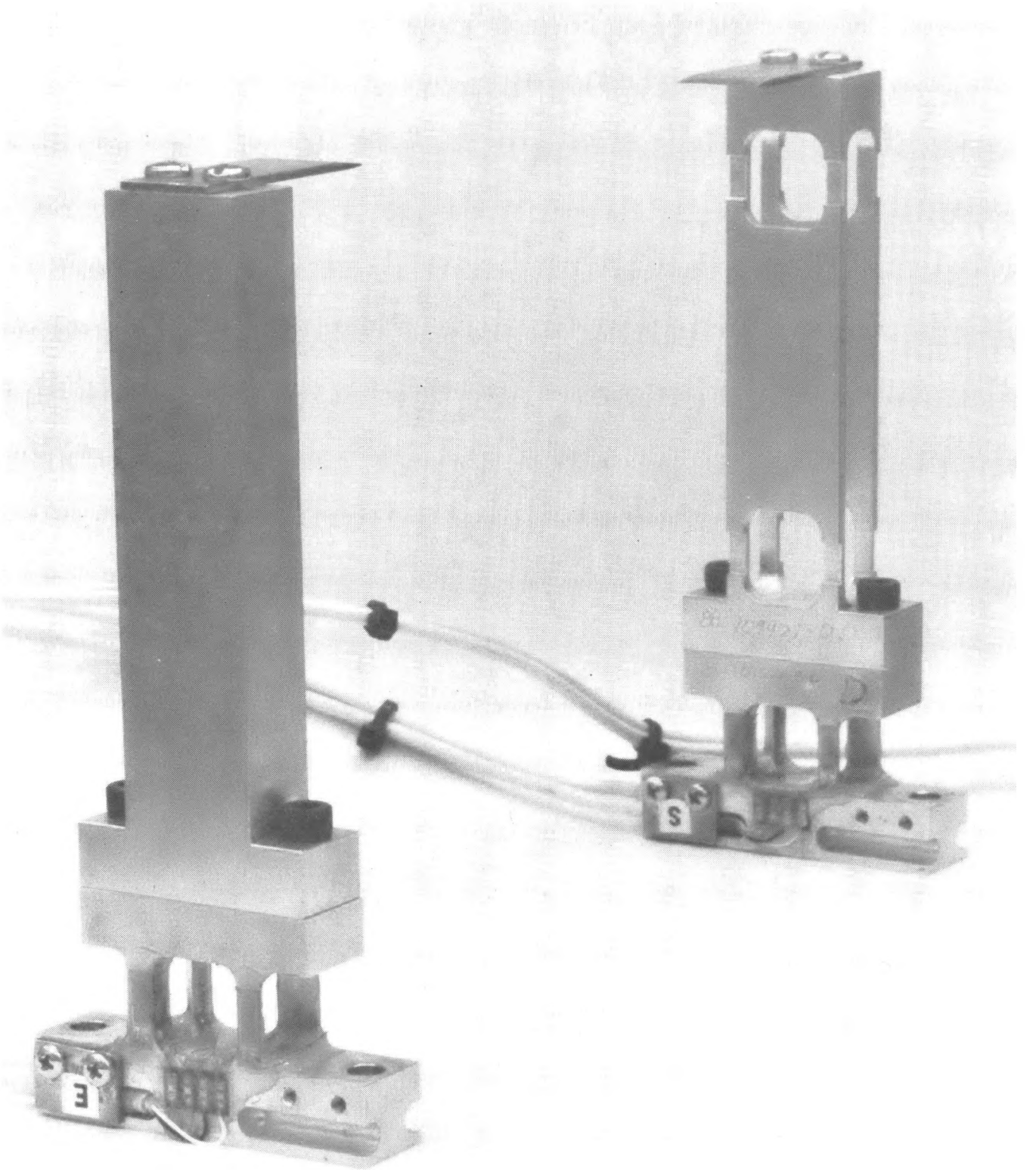

Figure 7. A photograph of the load cell in operation.

Table 1. Results of Spring Element Calculations

Applied force [Q] (lb)	Foot stress (psi)	Foot strain (in./in.)	Lateral deflection at pickle fork (in.)	Comments
0.02	13	.000001	.000014	Minimum resolution of 1 microstrain
0.10	65	.000005	.000070	Nominal lateral load
1.0	650	.000050	N/A	Nominal end load
20.0	13,000	.001000	N/A	Maximum expected overload

The minimum required resolution of 0.02 lb at 0.000001 strain is achieved. With a nominal working load of approximately 1.0 lb, we felt that 20 times this amount was a reasonable estimate for an overload. With 20 lbs applied, the resulting stress is 13,000 psi in the spring which is well below the yield point of 65,000 psi for 2024-T81 aluminum.

We were concerned that elastic lateral deflections would complicate our micropositioning task. These deflections would be due to the approximate 0.1 lb of force needed to overcome friction to translate (slide) a shelf sideways. The calculations show that a 0.1 lb lateral load results in a lateral deflection of only 0.000070 in. This is sufficiently small when compared to our positioning tolerance of ± 0.000250 in.

A foot area of 0.0064 in^2 results in a web thickness of 0.020 in. The final dimensions of the 90° angle, L-shaped feet were thus 0.170 in. × 0.170 in. × 0.020 in. thick × 0.600 in. tall. Simple buckling calculations had already predicted critical loads *greater* than the compressive load to yield. To prove the elastic stability of these elements, two sample parts were made of 6061-T6 aluminum (yield = 40,000 psi) and compressed until they buckled. The failure occurred at between 230-260 lb—results which agreed well with the calculated yield load of 250 lb Based on this experiment, the load cell can accept excessive loads that do not exceed the yield point of the spring material.

Conclusion

A unique, special-purpose load cell was designed for a precision assembly-operation where low deflections and high sensitivities to orthogonal forces were necessary. The hardware described was fabricated and found to work exceedingly well. It was used to support a major research program at LLNL.

When confronted with a seemingly unlimited array of design options, the author and his colleagues pursued a logical and systematic approach to arrive at a working and well-optimized solution. It is hoped that this synopsis of the design options and choices encountered in this project may prove useful to future designers of similar hardware.

Acknowledgments

I would like to thank Erni Halaxa and Bart Costerus for their able assistance with mechanical design issues and Maurice Hernandez, Bart Costerus, and Donald Roach for their valuable expertise in electrical design issues.

Also, Modern Strain Gage Transducers; Their Design and Construction is an excellent primer on strain gage technology.[2] I highly recommend it.

References

1. *Optimizing Strain Gage Excitation Levels*, Tech Note TN-502, Measurements Group, Inc., Raleigh, N. Carolina (1988).

2. *Modern Strain Gage Transducers; Their Design and Construction*, Micro-Measurements Division, Measurements Group, Inc., Raleigh, N. Carolina (1988).

Appendix A. Voltage Solution for the Wheatstone Bridge

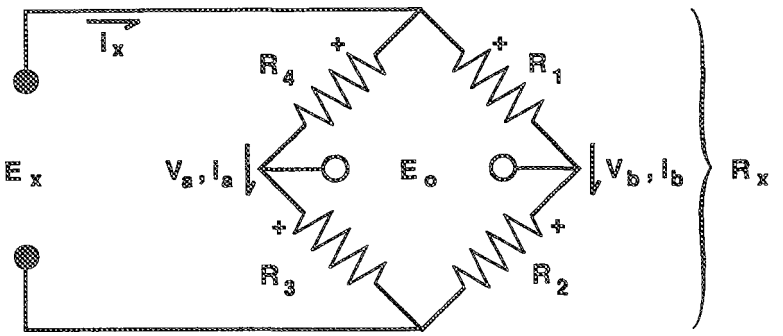

KNOWNS: E_x, $R_1 - R_4$,

UNKNOWNS: V_a, i_a, V_b, i_b, i_x, E_o, R_x

EQUATIONS (Seven equations for seven unknowns):

$$i_x = i_a + i_b \tag{1}$$

$$E_o = V_a - V_b \tag{2}$$

$$\frac{1}{R_x} = \frac{1}{(R_3 + R_4)} + \frac{1}{(R_1 + R_2)} \text{ (Resistances in parallel)} \tag{3}$$

$$i_x = \frac{E_x}{R_x} \tag{4}$$

$$V_a = i_a R_3 \tag{5}$$

$$V_b = i_b R_2 \tag{6}$$

$$-R_1 i_b - R_2 i_b + R_3 i_a + R_4 i_a = 0 \quad \text{(k's voltage law)} \tag{7}$$

SOLUTION

Use equation (3) to eliminate R_x in (4).

$$\frac{1}{R_x} = \left\{ \frac{1}{(R_3 + R_4)} + \frac{1}{(R_1 + R_2)} \right\} \tag{3}$$

$$\frac{1}{R_x} = \left\{ \frac{(R_1 + R_2) + (R_3 + R_4)}{(R_3 + R_4)(R_1 + R_2)} \right\} \tag{3}$$

$$\frac{1}{R_x} = \left\{ \frac{R_1 + R_2 + R_3 + R_4}{(R_3 + R_4)(R_1 + R_2)} \right\} \tag{3}$$

$$i_x = \frac{E_x}{R_x} = E_x \left(\frac{1}{R_x} \right) \tag{4}$$

$$i_x = E_x \left\{ \frac{R_1 + R_2 + R_3 + R_4}{(R_3 + R_4)(R_1 + R_2)} \right\} \tag{4}$$

Use (5) and (6) to eliminate V_a and V_b from (2).

$$V_a = i_a R_3 \tag{5}$$

$$V_b = i_b R_2 \tag{6}$$

$$E_o = V_a - V_b \tag{2}$$

$$E_o = i_a R_3 - i_b R_2 \tag{2}$$

Express (7) as i_a.

$$-R_1 i_b - R_2 i_b + R_3 i_a + R_4 i_a = 0 \tag{7}$$

$$i_b (-R_1 - R_2) + i_a (R_3 + R_4) = 0 \tag{7}$$

$$i_a (R_3 + R_4) = i_b (R_1 + R_2) \tag{7}$$

$$i_a = \frac{i_b(R_1 + R_2)}{(R_3 + R_4)} \tag{7}$$

Use (7) to eliminate i_a from (1).

$$i_x = i_a + i_b \tag{1}$$

$$i_x = i_b \frac{(R_1 + R_2)}{(R_3 + R_4)} + i_b \tag{1}$$

$$i_x = i_b \left\{ \frac{(R_1 + R_2)}{(R_3 + R_4)} + 1 \right\} \tag{1}$$

$$i_b = \frac{i_x}{\left\{ \frac{(R_1 + R_2)}{(R_3 + R_4)} + 1 \right\}} \tag{1}$$

Use (4) to eliminate i_x from (1).

$$i_x = E_x \left\{ \frac{R_1 + R_2 + R_3 + R_4}{(R_3 + R_4)(R_1 + R_2)} \right\} \tag{4}$$

$$i_b = \frac{E_x \left\{ \frac{R_1 + R_2 + R_3 + R_4}{(R_3 + R_4)(R_1 + R_2)} \right\}}{\left\{ \frac{(R_1 + R_2)}{(R_3 + R_4)} + 1 \right\}} \tag{1}$$

Use (7) to eliminate i_a from (2).

$$i_a = \frac{i_b(R_1 + R_2)}{(R_3 + R_4)} \tag{7}$$

$$E_o = i_a R_3 - i_b R_2 \tag{2}$$

$$E_o = \frac{i_b(R_1 + R_2)}{(R_3 + R_4)} R_3 - i_b R_2 \tag{2}$$

$$E_o = i_b \left\{ \frac{R_3(R_1 + R_2)}{(R_3 + R_4)} - R_2 \right\} \tag{2}$$

Use (1) to eliminate i_b from (2).

$$E_o = i_b \left\{ \frac{R_3 (R_1 + R_2)}{(R_3 + R_4)} - R_2 \right\} \tag{2}$$

$$E_o = \frac{E_x \left\{ \frac{R_1 + R_2 + R_3 + R_4}{(R_3 + R_4)(R_1 + R_2)} \right\}}{\left\{ \frac{(R_1 + R_2)}{(R_3 + R_4)} + 1 \right\}} \cdot \left\{ \frac{R_3 (R_1 + R_2)}{(R_3 + R_4)} - R_2 \right\} \tag{2}$$

For this application we wish to know $\frac{E_o}{E_x}$

$$\frac{E_o}{E_x} = \frac{\left\{ \frac{R_1 + R_2 + R_3 + R_4}{(R_3 + R_4)(R_1 + R_2)} \right\} \cdot \left\{ \frac{R_3 (R_1 + R_2)}{(R_3 + R_4)} - R_2 \right\} [R_3 + R_4]}{\left\{ \frac{(R_1 + R_2)}{(R_3 + R_4)} + 1 \right\} [R_3 + R_4]}$$

$$\frac{E_o}{E_x} = \frac{\left\{ \frac{R_1 + R_2 + R_3 + R_4}{(R_3 + R_4)(R_1 + R_2)} \right\} \cdot \left\{ R_3 (R_1 + R_2) - R_2 (R_3 + R_4) \right\}}{\{R_1 + R_2 + R_3 + R_4\}}$$

$$\frac{E_o}{E_x} = \frac{R_3 (R_1 + R_2) - R_2 (R_3 + R_4)}{(R_3 + R_4)(R_1 + R_2)}$$

For a strain gage application, we wish to know the change in E_o as a function of strain. The change in resistance for a single strain gage is

$\delta R = RG\varepsilon$

where:

δR = change in resistance (ohms)

R = nominal resistance (ohms)

G = gage factor (no units)

ε = strain (no units)

In a properly configured circuit, the nominal resistances will all be the same.

$R_1 = R_2 = R_3 = R_4 = R$

$$\frac{\delta E_o}{E_x} = \frac{(R + \delta R_3)(R + \delta R_1 + R + \delta R_2) - (R + \delta R_2)(R + \delta R_3 + R + \delta R_4)}{(R + \delta R_3 + R + \delta R_4)(R + \delta R_1 + R + \delta R_2)}$$

$$\frac{\delta E_o}{E_x} = \frac{(R + \delta R_3)(2R + \delta R_1 + \delta R_2) - (R + \delta R_2)(2R + \delta R_3 + \delta R_4)}{(2R + \delta R_3 + \delta R_4)(2R + \delta R_1 + \delta R_2)}$$

$$\frac{\delta E_o}{E_x} = \frac{(R + RG\varepsilon_3)(2R + RG\varepsilon_1 + RG\varepsilon_2) - (R + RG\varepsilon_2)(2R + RG\varepsilon_3 + RG\varepsilon_4)}{(2R + RG\varepsilon_3 + RG\varepsilon_4)(2R + RG\varepsilon_1 + RG\varepsilon_2)}$$

$$\frac{\delta E_o}{E_x} = \frac{(1 + G\varepsilon_3)(2 + G\varepsilon_1 + G\varepsilon_2) - (1 + G\varepsilon_2)(2 + G\varepsilon_3 + G\varepsilon_4)}{(2 + G\varepsilon_3 + G\varepsilon_4)(2 + G\varepsilon_1 + G\varepsilon_2)}$$

Perform the math to get the following:

$$\frac{\delta E_o}{E_x} = \frac{G\varepsilon_1 - G\varepsilon_2 + G\varepsilon_3 - G\varepsilon_4 + G^2\varepsilon_1\varepsilon_3 - G^2\varepsilon_2\varepsilon_4}{4 + 2G\varepsilon_1 + 2G\varepsilon_2 + 2G\varepsilon_3 + 2G\varepsilon_4 + G^2\varepsilon_1\varepsilon_3 + G^2\varepsilon_1\varepsilon_4 + G^2\varepsilon_2\varepsilon_3 + G^2\varepsilon_2\varepsilon_4}$$

In a properly configured bridge, all strains are of the same magnitude (ε_o) with the following sign relations:

$\varepsilon_1 = \varepsilon_3 = +\varepsilon_o$

$\varepsilon_2 = \varepsilon_4 = -\varepsilon_o$

This substitution results in significant simplification of the equation.

$$\frac{\delta E_o}{E_x} = \frac{G\varepsilon_o + G\varepsilon_o + G\varepsilon_o + G\varepsilon_o}{4} = \frac{4G\varepsilon_o}{4} = G\varepsilon_o$$

$\delta E_o = E_x G\varepsilon_o$

The accepted solution for a Wheatstone bridge with four active gages.

Appendix B. MicroEngineering 250BA-1000 Strain Gage

GAGE GEOMETRY ACTUAL SIZE	GAGE NUMBER	RESISTANCE IN OHMS	GRID LENGTH	GRID WIDTH	OVERALL LENGTH	OVERALL WIDTH
	250 BA-350	350 ± 0.5	.250"	.125"	.373"	.125"
			6.35mm	3.18mm	9.47mm	3.18mm
	250 BA-500	500 ± .75	.250"	.125"	.377"	.125"
			6.35mm	3.18mm	9.58mm	3.18mm
	250 BA-1000	1000 ± 2.0	.250"	.125"	.375"	.125"
			6.35mm	3.18mm	9.53mm	3.18mm
	250 BA-2000	2000 ± 4.0	.250"	.125"	.375"	.125"
			6.35mm	3.18mm	9.53mm	3.18mm
	250 BB-120	120 ± 0.5	.250"	.175"	.490"	.175"
			6.35mm	4.45mm	12.4mm	4.45mm
	250 GD-117	117 ± 0.5	.250"	.250"	.450"	.250"
			6.35mm	6.35mm	11.4mm	6.35mm
	250 GD-120	120 ± 0.5	.250"	.250"	.450"	.250"
			6.35mm	6.35mm	11.4mm	6.35mm
	250 GD-160	160 ± 0.5	.250"	.250"	.450"	.250"
			6.35mm	6.35mm	11.4mm	6.35mm

Appendix C. Transducer Spring Element Materials Selection Chart

MATERIAL DESIGNATION	PROPERTIES (in "as-normally-used" condition)*								RELATIVE *FIGURE OF MERIT* †										REMARKS
	Modulus of Elasticity, psi x 10^{-6} [1]	Yield Strength (0.2% offset) psi x 10^{-3} [2]	Thermal Expansion Coeff., ppm/°F [3]	Density, lb/in^3 [4]	Max. Recommended Temperature, °F [5]	Thermal Conductivity Btu / hr·ft^2·(°F/in) [6]	Elongation, % [7]	Hardness (Rc, unless noted)	Thermal Conductivity	Linearity	Hysteresis	Creep/Relaxation	Material Cost	Machinability	Hardening Distortion	Corrosion Resistance	Welding or Brazing Suitability	Lot-to-lot Consistency	
High-Modulus Alloys																			
4140	30	200	6.5	0.283	+400	270	12	42-45	3	8	8	7	9	5	3	1	5	6	very good alloy steel
E4340	30	210	6.3	0.283	+500	260	12	43-46	3	8	8	8	8	5	3	1	5	8	excellent alloy steel
18 Ni (250), maraging steel	27	245	5.6	0.289	+600	140	7-10	48-49	2	8	8	7	4	5	8	2	8	5	good, but seldom used
410 stainless	29	140	6.0	0.280	+400	170	15	39	2	7	7	6	7	4	2	6	2	6	seldom used
630 stainless (17-4 PH)	28.5	185	6.0	0.280	+400	135	14	41-44	2	7	7	7	6	6	8	7	7	3-4	widely used
631 stainless (17-7 PH)	29	220	5.7	0.276	+400	130	6-7	46-48	2	8	8	7	6	6	8	7	7	5	widely used
632 stainless (PH 15-7 Mo)	29	220	5.0	0.277	+500	110	6	47	2	8	8	8	4	6	8	7	7	5	excellent, but seldom used
S15500 stainless (15-5 PH)	28.5	185	6.0	0.280	+400	135	14	41-44	2	7	7	7	6	6	8	7	7	5-6	improved version of 630
Low-Modulus Alloys																			
2014-T6 alum.	10.6	60	12.4	0.101	+200	1075	10	B 135	8	6	7	6	5	8	9	3	3	6	good
2020-T4/T351 alum.	10.6	46	12.6	0.101	+200	840	18	B 120	7	6	7	6	5	8	9	3	3	6	good, widely used
2024-T81 alum.	10.6	65	12.6	0.101	+250	1040	8	B 128	8	7	8	7	5	8	9	3	3	6	best of aluminum alloys
6061-T6 alum.	10.0	40	12.9	0.098	+150	1160	14	B 95	8	5	4	4	6	7	8	4	5	5	fair performance
7075-T6 alum.	10.4	70	12.9	0.101	+100	840	10	B 150	7	7	6	6	5	8	8	3	2	5	poor at elevated temperatures
BeCu 25 alloy (C17200)	17	170	9.3	0.298	+250	750	2-3	40-42	7	8	8	8	2	5	9	3	4	7	excellent, but costly
6 Al-4V titanium alloy	16.5	165	4.9	0.160	+300	50	12	40	1	7	7	7	2	3	2	8	4	5	used in special applications only
Miscellaneous Materials																			
304 austenitic stainless	28	150	9.6	0.290	+250	110	4-5	39	2	5	4	4	7	3	–Ⓑ	8	5	6	poor spring material
Ni-SPAN-C alloy	28	180	4.3	0.294	+250	90	9	37-38	1	8	8	8	3	3	4	3	5	7	very good, but costly
AZ31 B magnesium alloy	6.5	32	14.5	0.064	+100	650	15	B 73	6	3	2	2	6	8	–Ⓑ	1	7	5	very poor spring material
Ceramic, Al_2O_3 (99+% pure)	55	60-70	3.3	0.141	+500	260	–Ⓐ	MOHS:9	3	7	8	8	1-3	1	–Ⓑ	10	–	7	special applications only
Epoxy-glass laminate (high-pressure, low resin content)	5-7	70-100	5-8	0.06-0.07	100-200	2	–	–	1	5	4	3	5	3	–Ⓑ	4	–	3	special, low-accuracy applications only

**The mechanical and physical properties given in this table have been carefully selected from a wide range of sources as representative for typical transducer applications and environments.*

†Numbers tabulated for FIGURE OF MERIT *represent relative ratings on a scale of 1 to 10, with higher numbers indicative of more desirable qualities. The ratings are based on experience, judgment, and current practices in the transducer field.*

[1] for GPa, multiply by 6.9
[2] for MPa, multiply by 6.9
[3] from 75°F to 212°F; for ppm/°C, multiply by 1.8
[4] for g/cm^3, multiply by 27.7
[5] transducer applications; for °C, subtract 32 and multiply by 5/9
[6] for watt/m·°C, multiply by 0.144
[7] in 2 in, or 51 mm

Ⓐ no ductile range
Ⓑ not hardenable by heat treatment

Appendix D. Load Cell Performance Calculations

To properly evaluate all of the variables involved, it is best to have a deflection and strain model. See Figure below.

Letter

- Q Lateral load applied by shelf (lbs)
- Y Lateral deflection by beam calculation (in.)
- S Lateral deflection by shear calculation (in.)
- L Length measurement (height)
- W Width measurement
- T Thickness measurement
- F Vertical load per load cell column
- E Young's modulus
- G Shear modulus
- P Lateral load per cell column
- A Area
- R Swing displacement due to "Rθ"
- X Distance between vertical columns of load cell
- D Total lateral deflection at top of arm

Subscript

- a (Zone a) The arm
- b (Zone b) The spring element
- c (Zone c) The base

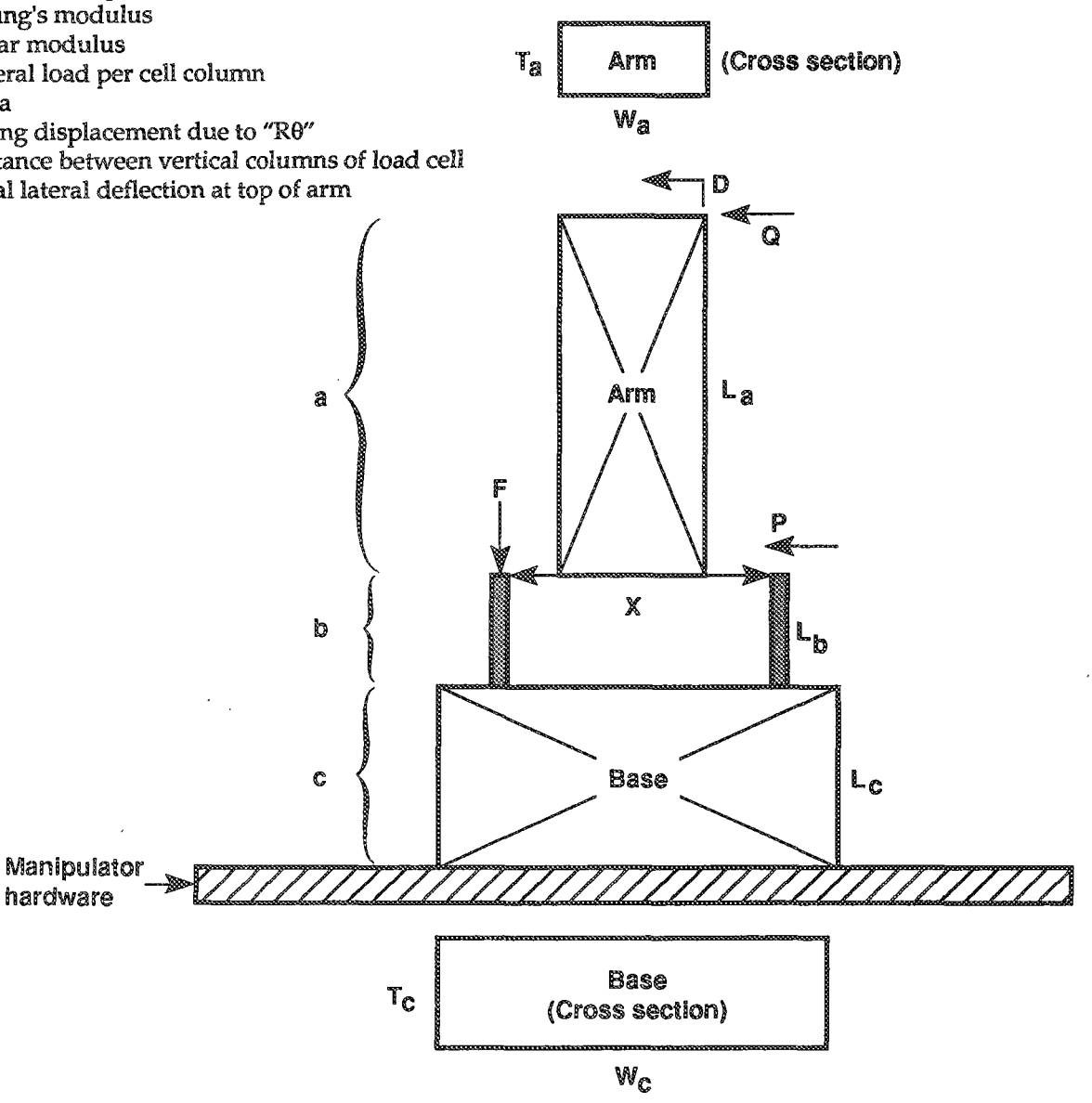

Zone a – The Arm

The lateral deflection is calculated as a beam:

$$Y = \frac{WL^3}{3EI} = \frac{Q \cdot (L_a)^3}{3\, E_a\, I_a} = Y_a$$

$$I_a = \frac{1}{12} T_a\, (W_a)^3$$

Zone b – The Spring Element

We first calculate the vertical force on each of the four (4) columns of the spring element due to Q:

$$(2F)\,(X) = Q\, L_a$$

$$F = \frac{Q\, L_a}{2\, X}$$

Lateral deflection due to shear for these short elements:

$$P = \frac{Q}{4}$$

$$S_b = \frac{F\, L}{A\, G} = \frac{P\, L_b}{A_b\, G_b}$$

During loading the compressed columns get shorter and the tensioned columns get taller. This results in an "R • θ" swing arm displacement.

Deflection at top of arm is calculated as:

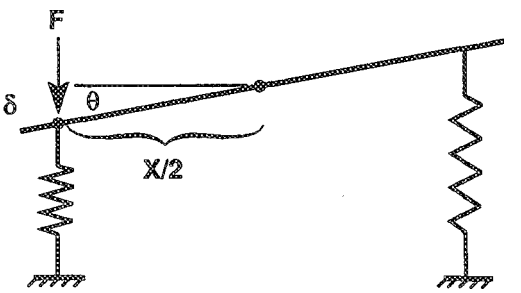

$$\theta = \frac{\delta}{\left(\frac{X}{2}\right)} = \frac{\left(\frac{FL}{EA}\right)}{\left(\frac{X}{2}\right)} = \frac{\left(\frac{F L_b}{E_b A_b}\right)}{\frac{X}{2}}$$

$$\theta = \frac{2 F L_b}{X E_b A_b}$$

$$R = L_a \theta = \frac{2 F L_a L_b}{X E_b A_b}$$

Stress and strain in a single vertical column of the spring element due to Q

$$\text{Strain} = \frac{F}{AE} = \frac{F}{A_b E_b}$$

$$\text{Stress} = \frac{F}{A} = \frac{F}{A_b}$$

From the voltage solution for a Wheatstone bridge, we know that output voltage is the product of gage factor, strain, and excitation voltage.

$$E_o = Gf \cdot \text{Strain} \cdot E_X$$

Zone c – The Base

Lateral deflection of the base due to shear:

$$S_c = \frac{FL}{AG} = \frac{Q L_c}{A_c G_c}$$

$$A_c = T_b W_b$$

The total deflection at the top of the arm is the sum of following terms:

$$D = Y_a + S_b + R + S_c$$

Table D-1. Spreadsheet Calculations for Load Cell Performance.

Deflection and Strain Model

Note: All units are English.

E, G (psi)
L, T,W,S,R,Y (in.)
A ($in.^2$)
Q,F,P (lb)
I ($in.^4$)
THETA (radian)
E_X,E_O (v)

Zone a		Zone b		Zone c	
Inputs					
Ea	10.6E+06	Eb	10.6E+06	Ec	10.6E+06
Ga	4.0E+06	Gb	4.0E+06	Gc	4.0E+06
La	5.0	Lb	0.6	Lc	2.0
Ta	0.5			Tc	1
Wa	1.2	Ab	0.0064	Wc	2
		X	0.6		
Q	0.02	G*f*	2		
		Ex	10		
Outputs					
Ia	0.0720	F	0.0833333333	Ac	2
		P	0.005		
		THETA	0.00000246		
		Foot Stress	13.020833		
		Foot Strain	0.000001228		
		Eo	0.000025		
Ya	0.0000011	Sb	0.0000001	Sc	0.00000000
				R	0.0000123

Total End Deflection D = Ya + Sb + R +Sc = 0.0000135 in.